Proceedings of the Thirty-fourth (2024) International Ocean and Polar Engineering Conference
Rhodes, Greece, June 16–21, 2024

Finite Element Analysis of Lateral Soil Reaction of Monopile in Sand Considering Effects of Pile Installation Process

Yayoi Ishii and *Kenji Shimada*
Institute of Technology, Shimizu Corporation
Koto-ku, Tokyo, Japan

Takeshi Ishihara
Department of Civil Engineering, The University of Tokyo
Bunkyo-ku, Tokyo, Japan

ABSTRACT

Simple formulae for calculating the soil moduli for the HSsmall model based on the CPT cone resistance are proposed for the monopile foundation of a bottom-fixed-type offshore wind turbine in sand. The pile responses predicted by the proposed formulas show good agreement with the responses obtained from the field loading tests and centrifuge model tests. It is found that pile responses can be reproduced by using a unique interface strength reduction factor of $R_{inter} = 0.6$ regardless of installation process, such as impact driving in field loading tests, and 1-g state jacking in centrifuge model tests.

KEY WORDS: Monopile; CPT; Soil moduli; Interface strength reduction factor; 3D Finite element analysis; HSsmall; PLAXIS 3D.

NOMENCLATURE

c' : Effective cohesion (kPa)
D : Pile diameter (m)
E : Modulus of elasticity of pile material (kPa)
E_{50} : Secant soil modulus at half of soil strength (kPa)
E_i : Young's modulus of interface (kPa)
E_s : Young's modulus of soil (kPa)
E_s^{inc} : Increase of Young's modulus with depth (kPa/m)
E_s^{ref} : Young's modulus of soil corresponding to the reference depth z_{ref} (kPa)
EI : Flexural rigidity of pile (kNm^2)
E_{oed} : Oedometer soil modulus (kPa)
E_{ur} : Unloading/reloading soil modulus(kPa)
E_{50}^{ref} : Reference secant soil modulus at half of soil strength corresponding to the reference confining pressure p_{ref} (kPa)
E_{oed}^{ref} : Reference oedometer soil modulus corresponding to the reference confining pressure p_{ref} (kPa)
E_{ur}^{ref} : Reference unloading/reloading soil modulus corresponding to the reference confining pressure p_{ref} (kPa)
G_0 : Small strain shear modulus (kPa)
G_0^{ref} : Reference small strain shear modulus corresponding to the reference confining pressure p_{ref} (kPa)
h : Loading height (kN)
H : Horizontal load (kN)
I : Area moment of inertia of pile (m^4)
K_0 : Coefficient of lateral earth pressure (-)
L : Embedded length of pile (m)
m : Power for stress-level dependency of stiffness (-)
M : Bending moment of pile (kNm)
p_{ref} : Reference confining pressure (kPa)
q_c : CPT cone resistance (kPa)
q_c^* : Dimensionless CPT cone resistance (-)
RD : Relative density (%)
R_f : Failure ratio (-)
R_{inter} : Interface stiffness reduction factor (-)
t : Pile thickness (mm)
y : Displacement of pile at depth z (m)
y_g : Ground-level displacement of pile (m)
z : Depth below the ground surface(m)
z_{ref} : Reference depth (m)
α : Coefficients of Eq. 13 representing the relationship between q_c(kPa) and E_s(kPa) (-)
γ_{sat} : Saturated unit weight (kN/m^3)
$\gamma_{0.7}$: The strain level at which the shear modulus G has reduced to about 70% of the small-strain shear modulus G_0 ($G/G_0 = 0.7$) =$0.385\gamma_{0.5}$ (-), where $\gamma_{0.5}$ is the strain level at $G/G_0 = 0.5$(-)
ν : Poisson's ratio of soil for small strain (HSsmall) (-)
ν_s : Poisson's ratio of soil (-)
ν_i : Poisson's ratio of interface (-)
ϕ' : Friction angle (degree)
σ_{11} : Major principal stress (kPa)
σ'_{v0} : Initial vertical effective stress (kPa)
σ'_3 : The minor principal stress of soil (kPa)

τ_{lim} : Shear strength of soil (kPa)
$\tau_{lim,i}$: Shear strength of interface element (kPa)
ψ : Dilatancy angle of soil (degree)

INTRODUCTION

The soil reaction characteristics required for the design of monopiles are usually obtained by 3D FEA. It is important how to determine the appropriate geotechnical parameters for the constitutive laws used in the 3D FEA based on the results of the geotechnical investigation. Cone resistance of the cone penetration test (CPT) has been used to evaluate the relationship between various soil strength properties and soil stiffness (Robertson and Cabal, 2022; Igoe 2020, 2022). CPT has been used not only in field loading tests but also in centrifuge model tests where cone resistance has been measured using miniature CPT with centrifugal forces acting during centrifuge flights (Haouari and Bouafia, 2020; Fan et al., 2019). However, to the authors' knowledge, there are no convenient formulae that can be applied in both field loading tests and centrifuge model tests to obtain the soil stiffness parameters in 3D FEA from the CPT cone resistance.

Modeling of the pile-soil interface is important for the analysis of monotonic loading. In the case of field loading tests, the test piles are generally installed by impact driving with hydraulic hammers, as in the case of actual piles. On the other hand, in the centrifuge model test, the model pile is jacked into the soil. Since the soil near the piles is disturbed by the installation of the piles, some treatment of the pile-soil interface is required in the FE analysis. Fan et al. (2021) investigated numerically by employing coupled Eulerian–Lagrangian (CEL) method, in which rigorously simulated installation process. In FEA, an interface element is often set up between the pile and the surrounding soil. There are two approaches for setting the strength and stiffness of the interface element: one is to estimate them by laboratory tests, and the other is to simply reduce the strength and stiffness of the surrounding soil. As the former, for example, Nakamura et al. (2023) estimated the strength and stiffness by laboratory tests using remolded samples, while Pedone et al. (2023) estimated the strength from laboratory tests and determined the stiffness by sensitivity studies. The latter method reduces the strength and stiffness of the surrounding soil by the interface strength reduction factor R_{inter} (PLAXIS 3D, 2023), and this method is employed in this study.

In latter method, the interface strength reduction factor R_{inter} should be set appropriately according to installation process. However, there are few studies on how to set the interface strength reduction factor R_{inter}.

In this study, an overview of the existing field loading tests and centrifuge model tests is provided, and the HSsmall modeling in PLAXIS 3D is described. A set of simple formulae for estimating soil moduli for the HSsmall model based on the CPT cone resistance are then proposed. The applicability of the proposed formulae and the interface strength reduction factor for the pile-soil interface is discussed. Finally, conclusions from this study are presented.

OVERVIEW OF FIELD LOADING TEST AND CENTRIFUGE MODEL TESTS AND ANALYSIS METHOD

Overview of field loading tests and centrifuge model tests

Table.1 lists the field loading tests and centrifuge model tests that are subjected to the analysis, as well as the main specifications of the test piles and the relative densities of the sandy soil bed. The analyses are performed on one field loading test (PISA (Byrne et al., 2017; Zdravković et al., 2020; Taborda et al., 2020; Burd et al., 2020; Minga and Burd, 2019; McAdam et al., 2020) as shown in Case P) and two centrifuge model tests (Haouari and Bouafia, 2020 as shown in Case H and Fan et al., 2019 as shown in Case F). In all tests as shown in Table.1, cone penetration tests (CPT) were performed to investigate soil properties.

The surfaces of the model piles used in the centrifuge model tests are smooth in Case F, but roughened with bonded sand in Case H. In all cases, the piles were installed by jacking in the 1-g condition. In Case F, *n*-g state jacking, i.e., penetration by jacking during flight, was also performed, however, it is excluded from this study because it requires special centrifuge equipment.

In the field test, Case P was impact driving with a hydraulic hammer, but the first 1 to 1.5 m embedment was reported to be vibro-hammered (McAdam et al., 2020).

Overview of 3D FEA and Interface Elements

3D FEA are performed using PLAXIS 3D (Version 2023.2) and PLAXIS Monopile Designer (Version 2023.2) by the effective stress analysis under the drained condition. Fig. 1 shows an example of numerical model. The depth profiles of displacements and bending moments in the piles are obtained as the average values of dummy beams (see Fig. 1) placed in front and behind the piles with very small stiffness.

The HSsmall model (Schanz et al., 1999; Benz, 2007; PLAXIS 3D, 2023) is used in this study, which is a standard model of PLAXIS and is also used in the PISA project as the constitutive law for the sandy soil. The soil stiffness parameters required by the model are obtained by considering the confining pressure using the following equation,

Table.1 Pile structural properties and soil relative densities for analyses of the monotonic loading.

	PISA (2017, 2019, 2020)	Haouari and Bouafia (2020)		Fan et al. (2019)
Test	Field test	Centrifuge (17.85, 20 G)		Centrifuge (100 G)
Test site	Dunkirk	IFSTTAR		C72
Case No.	P	H1	H2	F
Aspect ratio L/D	5.25	10	5.56	3.1
Diameter D (m)	2	0.5	0.9	5.22
Embedded length L (m)	10.57	5		16.2
Pile thickness t (mm)	38	21.7	44.8	21
Loading height h (m)	9.89	1		19.8
EI (MN/m^2)	23676	56.65	740.9	924400
Pile surface finish	Rusted	Roughened with bonded sand		Smooth
Installation	Vibro (1 to 1.5 m) +Impact Driving	1-g Jacking		1-g Jacking
Relative density RD (%)	75 %, 100 % (Dunkirk sand)	92 % (Le-Rheu sand)		38 % (UWA silica sand)

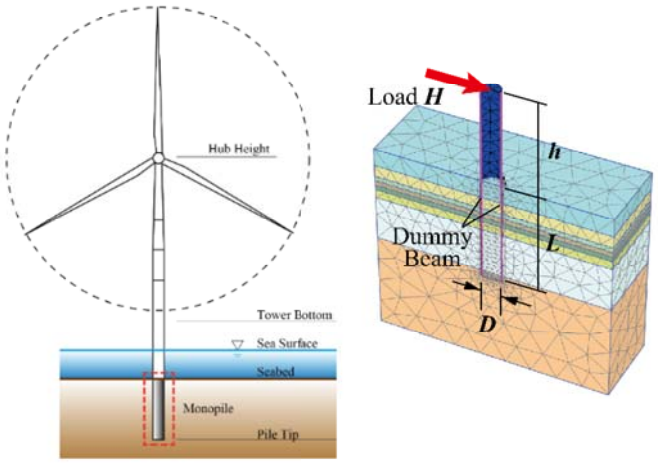

Fig. 1 FEA model and dummy beams.

$$E(z) = E^{ref}\left(\frac{c' + |\sigma'_3|\tan\phi'}{c' + p_{ref}\tan\phi'}\right)^m \quad (1)$$

where c' is the effective cohesion (kPa), σ'_3 is the minor principal stress (kPa), ϕ' is the internal friction angle (deg), m is the power index which expresses the constrained stress dependency and of 0.5, p_{ref} is the reference stress of 100 (kPa), $E(z)$ is the various soil moduli (E_{50} is the secant soil modulus at half of soil strength, E_{ur} is the unloading-reloading soil modulus, E_{oed} is the oedometer soil modulus) below z(m) from ground surface and E^{ref} is $E(z)$ at reference stress p_{ref}. E_{oed} and E_{ur} are obtained from following equations,

$$E_{oed} = E_{50} \quad (2)$$

$$E_{ur} = 3E_{50} \quad (3)$$

Interface elements are used at the interface between the pile and the soil, with normal and shear stresses approximated by a bilinear model. In this study, to ensure that the 3D FEA results match the field loading tests and centrifuge model tests, the strength $\tau_{lim}(= c' + \sigma'_3\tan\phi')$ and stiffness of the surrounding soil are reduced with the interface strength reduction factor R_{inter} to obtain the interface element strength $\tau_{lim,i}$ and shear modulus G_i and oedometer modulus $E_{oed,i}$,

$$\tau_{lim,i} = R_{inter} \cdot \tau_{lim} \quad (4)$$

$$G_i = R_{inter}^2 \frac{E_s}{2(1+\nu_s)} = R_{inter}^2 G_s \quad (5)$$

$$E_{oed,i} = \frac{E_i(1-\nu_i)}{(1+\nu_i)(1-2\nu_i)} \quad (6)$$

where, E_i and ν_i are the soil modulus and the Poisson's ratio of the interface element, $E_i = 2(1+\nu_i)G_i$ and $\nu_i = 0.45$, respectively. In addition, G_s and E_s are used in the bilinear model for the interface elements and are obtained as $G_s = E_s/2(1+\nu_s)$ and E_s is approximated linearly with depth and is described below,

$$E_s(z) = E_s^{inc}\left(z - z_{ref}\right) + E_s^{ref} \quad (7)$$

where E_s^{ref} and E_s^{inc} are Young's modulus of soil corresponding to the reference depth z_{ref} and increment of Young's modulus with depth (kPa/m), respectively.

The Poisson's ratio ν used in the HSsmall model is $\nu = 0.17$ for Case P (Zdravković et al., 2020) and $\nu = 0.2$ (Mayne et al., 2009) for the centrifuge model tests (Case H and Case F). Poisson's ratio ν_s is 0.3. Failure ratio R_f and the strain level $\gamma_{0.7}$ at which the shear modulus G has reduced to about 70% of the small-strain shear modulus G_0 are approximated using conversion formulae in terms of relative density RD (%) by Brinkgreve et al. (2010),

$$R_f = 1 - RD/800 \quad (8)$$

$$\gamma_{0.7} = \left(2 - \frac{RD}{100}\right)\cdot 10^{-4} \quad (9)$$

In addition, according to the PLAXIS 3D specification, if $R_{inter} \neq 1$, the dilatancy angle of the interface element is set to 0.

PROPOSE OF SOIL MODULI BASED ON CPT CONE RESISTANCE

Correlations between the small strain shear modulus G_0 and cone resistance q_c was developed by several researchers. Baldi et al. (1981) performed triaxial tests for normally consolidated, uncemented, quartz sands. Robertson and Campanella (1983) demonstrated $G_0 - q_c$ relationship for different initial vertical effective stresses σ'_{v0}. Rix and Stokoe (1991) considered variations of sand specimen and proposed average $G_0/q_c - q_c/\sqrt{\sigma'_{v0}}$ relationship.

Baldi et al. (1981) developed estimation formulae for E_{50}, however, it is not correlated with q_c. Robertson and Campanella (1983) established $E_{50} - q_c$ relationship for different initial vertical effective stresses σ'_{v0}. E_{50} is the dominant parameter in FEA using HSsmall, but no correlation formulae have been proposed.

In this study, simple formulae for calculating soil moduli G_0 and E_{50} for the HSsmall model based on the CPT cone resistance are proposed based

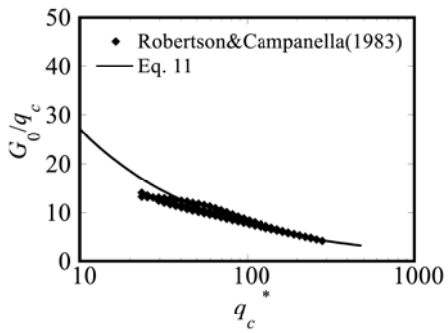

Fig.2 Correlation between q_c^* and G_0/q_c.

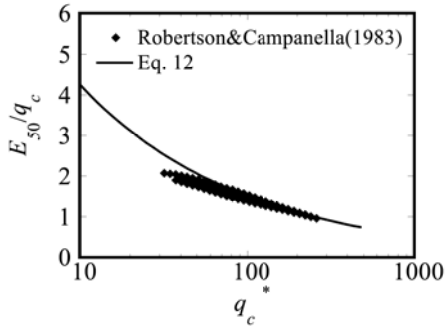

Fig. 3 Correlation between q_c^* and E_{50}/q_c.

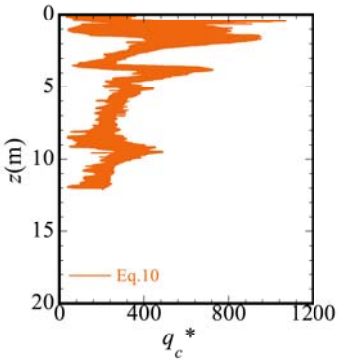

(a) Dimensionless CPT cone resistance q_c^*.

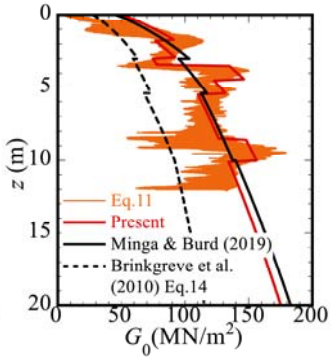

(b) Small-strain shear modulus G_0.

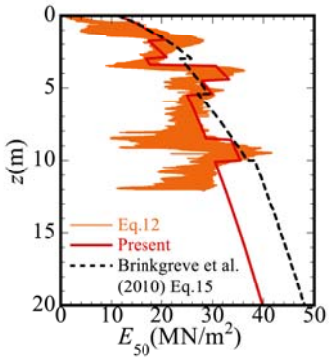

(c) Secant soil modulus at half of soil strength E_{50}.

Fig. 4 Vertical profiles of q_c^*, G_0 and E_{50} for Case P.

on Robertson and Campanella (1983) as follows.
Referring to Rix and Stokoe (1991), dimensionless cone resistance q_c^* is defined in terms of initial vertical effective stress σ'_{v0} as follows:

$$q_c^* = \left(\frac{q_c}{p_{ref}}\right) \cdot \left(\frac{\sigma'_{v0}}{p_{ref}}\right)^{-0.5} \tag{10}$$

Fig.2 shows $q_c^* - G_0/q_c$ correlation. It can be found that $q_c^* - G_0/q_c$ for different σ'_{v0} are estimated by a unique curve. In this study, G_0/q_c is expressed in terms of the dimensionless cone resistance q_c^* as follows:

$$\frac{G_0}{q_c} = 96 q_c^{*-0.55} \tag{11}$$

Similarly, for E_{50} (Fig.3), E_{50}/q_c is expressed as:

$$\frac{E_{50}}{q_c} = 12 q_c^{*-0.45} \tag{12}$$

The shear modulus of the surrounding soil for the interface element of the bilinear model is obtained from the following equation,

$$E_s = \alpha q_c \tag{13}$$

Since sandy soil is concerned in this study, $\alpha = 3$ is used (Haouari and Bouafia, 2020; Trofimenkov, 1974).

RESULTS AND DISCUSSION

Validation by field loading test

Fig. 4 shows the profiles of q_c^*, G_0 and E_{50} for Case P. The same figure also shows a comparison by the following conversion formulae (Brinkgreve et al., 2010) in terms of relative density RD (%),

$$G_0^{ref} = 60000 + 68000RD/100 \tag{14}$$

$$E_{50}^{ref} = 60000RD/100 \tag{15}$$

Because filed tests site is not composed of clean sand, q_c^* varies with depth significantly. G_0 based on Eq.11 also varies with depth, however averaged values represented by red line shows a good agreement with Zdravković et al. (2020) and Minga and Burd (2019) (Fig. 4(b)). On the other hand, although the formula of Brinkgreve et al. (2010) as in Eq. 14 underestimates G_0 and E_{50} by Eq. 15 as shown in Fig. 4(c) looks overestimated E_{50} in deep portion, however, shows a good agreement with proposed Eq. 12 in shallow depth.

Table 2 summarizes HSsmall soil parameters for Case P. Following Minga and Burd (2019), an artificial cohesion is considered for layers

Table 2 Soil parameters for HSsmall model (Case P).

Layer No.	Unit	1	2	3	4	5	6	7	8	9
z_{top}	m	0	1.8	3	3.5	4	4.5	5.4	8.5	10
z_{bottom}	m	1.8	3	3.5	4	4.5	5.4	8.5	10	20
z_{ref}	m	0	1.8	3	3.5	4	4.5	5.4	8.5	10
γ_{sat}	kN/m^3	17.1	17.1	17.1	17.1	17.1	17.1	19.9	19.9	19.9
c'	kPa	5	5	10	10	10	10	0.1	0.1	0.1
ϕ	°	46	46	42	42	42	42	42	42	42
ψ	°	17.5	17.5	12.5	12.5	12.5	12.5	12.5	12.5	12.5
G_0^{ref}	kPa	230000	190000	140000	240000	240000	200000	180000	210000	180000
E_{50}^{ref}	kPa	52273	43182	31818	54545	54545	45455	40909	47727	40909
E_{ur}^{ref}	kPa	156818	129545	95455	163636	163636	136364	122727	143182	122727
E_s^{ref}	kPa	0	135000	56471	30000	135000	105000	90000	54000	75000
E_s^{inc}	kPa/m	25000	-21814	-17647	70000	-20000	-5556	-3871	14667	0
$\gamma_{0.7}$	—	0.0001	0.0001	0.000125	0.000125	0.000125	0.000125	0.000125	0.000125	0.000125
RD	%	100	100	75	75	75	75	75	75	75
K_0	—	0.4	0.4	0.4	0.4	0.4	0.4	0.4	0.4	0.4
ν	—	0.17	0.17	0.17	0.17	0.17	0.17	0.17	0.17	0.17
ν_s	—	0.3	0.3	0.3	0.3	0.3	0.3	0.3	0.3	0.3
ν_i	—	0.45	0.45	0.45	0.45	0.45	0.45	0.45	0.45	0.45
R_f	—	0.875	0.875	0.90625	0.90625	0.90625	0.90625	0.90625	0.90625	0.90625

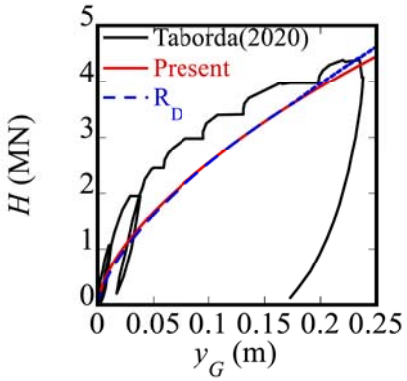

(a) $H - y_g$ relationship.

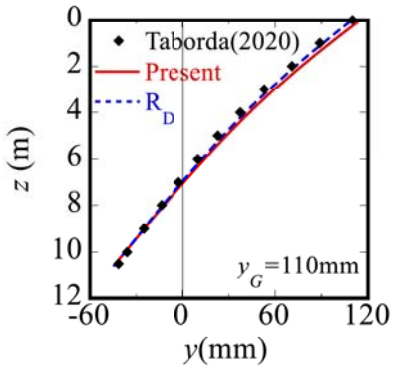

(b) Displacement.

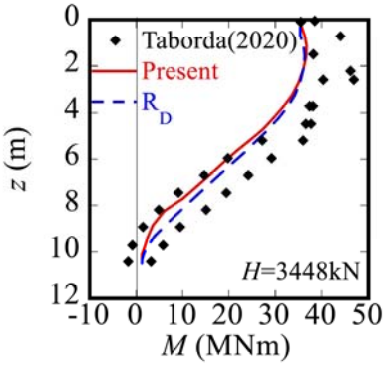

(c) Bending moment.

Fig. 5 Comparison between 3D FEA and measurements for Case P.

above the ground water level of $z = 5.4$ m to account for the unsaturated conditions. Interface strength reduction factor of $R_{inter} = 0.6$, which is commonly used for steel-sand interface (Gouw, 2014), is applied in the rest of this study regardless of installation process.

Fig. 5 shows a comparison between 3D FEA and field test results for the $H - y_g$ relationship, where H is horizontal load and y_g is ground-level displacement of pile, and the profiles of pile displacement and bending moment for the impact-driven pile Case P. Proposed formulae (Eqs. 11 and 12) give responses in good agreements with the measurements. Although G_0 is significantly underestimated, these agreements are also accomplished by Brinkgreve's formulae (Eqs. 14 and 15), which are based on the relative density. This would indicate that E_{50} is more dominant in the response than G_0, especially its shallower portion.

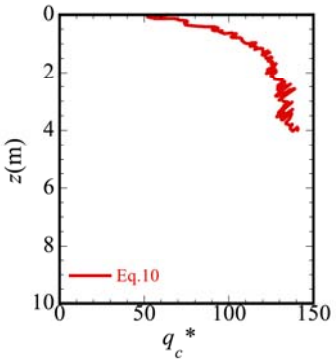

(a) Dimensionless CPT cone resistance q_c^*.

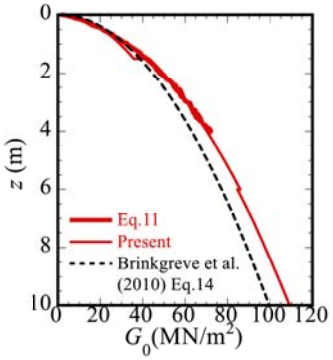

(b) Small-strain shear modulus G_0.

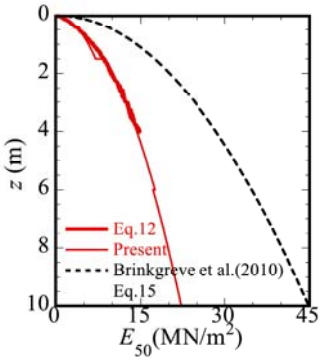

(c) Secant soil modulus at half of soil strength E_{50}.

Fig. 6 Vertical profiles of q_c^*, G_0 and E_{50} for Case H.

Although the proposed equation is for clean sand, it can be shown to be applicable to field tests by formulating the stiffness in terms of q_c^* rather than simply q_c.

Validation by centrifuge model tests

In this section, three centrifuge tests, that is applicability to different aspect ratio by Cases H1 and H2, to different relative density by Case F, are examined to validate the application of proposed soil moduli formulae and reduction factor of $R_{inter} = 0.6$.

Table 3 Soil parameters for HSsmall model (Case H).

Layer No.	Unit	1	2	3
z_{top}	m	0	1.5	6
z_{bottom}	m	1.5	6	15
z_{ref}	m	0	1.5	6
γ_{sat}	kN/m³	16.5	16.5	16.5
c'	kPa	0.1	0.1	0.1
ϕ	°	42	42	42
ψ	°	12	12	12
G_0^{ref}	kPa	113509	136464	134386
E_{50}^{ref}	kPa	22307	27803	27276
E_{ur}^{ref}	kPa	66921	83409	81828
E_s^{ref}	kPa	0	13150	30580
E_s^{inc}	kPa/m	13000	4710	1670
$\gamma_{0.7}$	—	0.000108	0.000108	0.000108
RD	%	92	92	92
K_0	—	0.4	0.4	0.4
ν	—	0.2	0.2	0.2
ν_s	—	0.3	0.3	0.3
ν_i	—	0.45	0.45	0.45
R_f	—	0.885	0.885	0.885

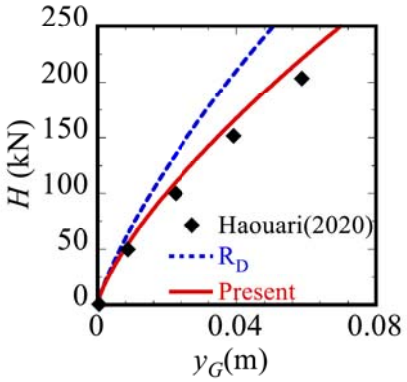

(a) $H - y_g$ relationship.

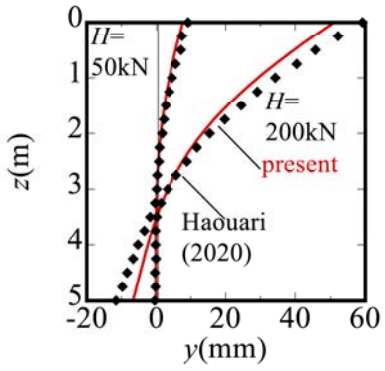

(b) Displacement.

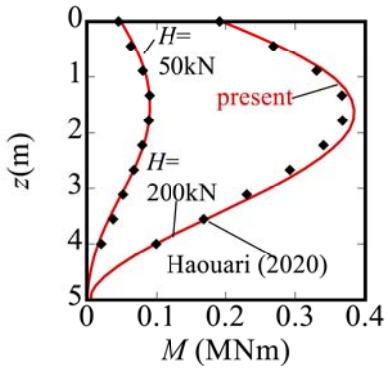

(c) Bending moment.

Fig. 7 Comparison between 3D FEA and measurements for Case H1.

At first, applicability to different aspect ratio, that is $L/D = 10$ for Case H1 and L/D =5.6 for Case H2, is discussed. Fig. 6 shows the soil profiles of q_c^*, G_0 and E_{50} for Case H. The same figure also shows a comparison of the conversion formulae (Brinkgreve et al., 2010) in terms of relative density RD (%). In Fig. 6 (a), compared to field test of Case P (Fig.4(a)), value and variation of q_c^* are small. Estimation by RD (Eqs. 14, 15) gives comparable profile for G_0 (Fig. 6 (b)), however, significant overestimation of E_{50} (Fig. 6 (c)) compared to those obtained by q_c^* (Eqs. 11, 12). Table 3 summarizes HSsmall soil parameters for Case H.

Fig. 7 shows a comparison between 3D FEA and centrifuge model tests for $H - y_g$ relationship and the profiles of pile displacement and bending moment for Case H1 pile ($L/D = 10$) of 1-g jacking. Proposed formulae (Eq. 11 and 12) yield responses in good agreement with the

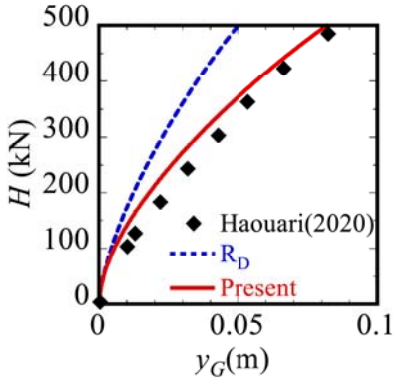

(a) $H - y_g$ relationship.

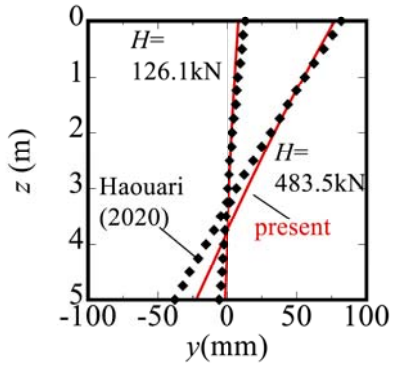

(b) Displacement.

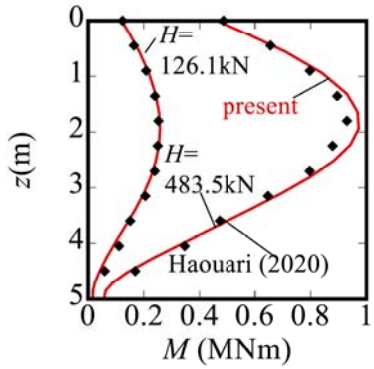

(c) Bending moment.

Fig. 8 Comparison between 3D FEA and measurements for Case H2.

measurements.

Combining the proposed soil moduli formulae with the reduction factor $R_{inter} = 0.6$, commonly used for impact driving in field tests, also successfully gives the response of 1-g jacking in centrifuge model tests.

On the other hand, when G_0 and E_{50} are determined based on relative density, the load is significantly overestimated (Fig.7(a)).

Even in more rigid pile case of H2 (L/D =5.6), Fig. 8 demonstrates that similar to Case H1, the combination of the proposed formulae and $R_{inter} = 0.6$ shows good agreement with the measurements.

Next, applicability to smaller relative density is examined for Case F of

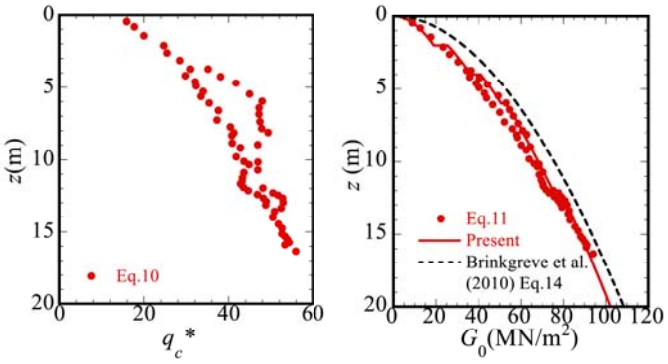

(a) Dimensionless CPT cone resistance q_c^*. (b) Small-strain shear modulus G_0.

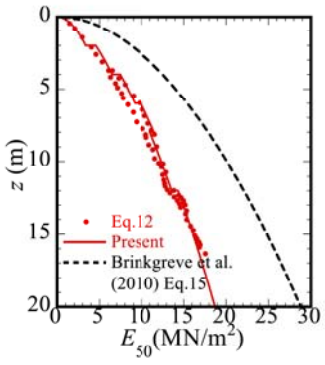

(c) Secant soil modulus at half of soil strength E_{50}.

Fig. 9 Vertical profiles of q_c^*, G_0 and E_{50} for Case F.

L/D =3.1 and RD =38%. In Fig. 9 (a), range of q_c^* is smaller than 60. It is worth to note that although some variation of q_c^* is observed in Fig. 9 (a), application of the proposed soil moduli formulae reduces the variation (Figs. 9 (b) and (c)). Table 4 summarizes HSsmall soil parameters for Case F.

Even in the case with a significantly small relative density of RD =38%, combination of the proposed soil moduli formulae and the reduction factor of $R_{inter} = 0.6$ shows good agreement with the measurements obtained from centrifuge model tests as shown in Fig. 10.

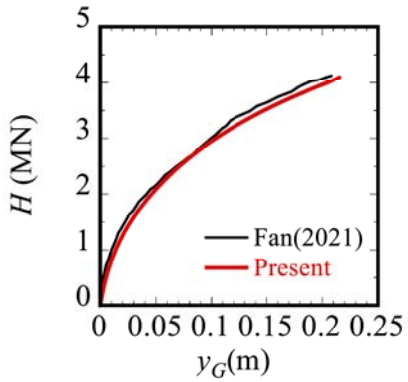

Fig. 10 $H - y_g$ relationship for Case F.

Fig. 11 demonstrates a comparison of the distribution of the major principal stress σ_{11} (kPa) in the loading direction at $y_G/D = 0.04$ between Fan et al. (2021) and the 3D FEA in this study. 3D FEA using PLAXIS 3D with the proposed formulae and $R_{inter} = 0.6$ shows favorable agreement with the analysis by Fan et al. (2021) employing coupled Eulerian–Lagrangian (CEL) method, in which installation process by 1-g jacking is rigorously simulated.

CONCLUSION

Simple formulae to calculate soil moduli (G_0 and E_{50}) are proposed for monopile foundations of bottom-fixed offshore wind turbines in sand, and 3D FEA using HSsmall model for monotonic loading of piles is performed. The following conclusions are obtained.

1. Simple formulae for calculating small strain shear modulus G_0 and secant soil modulus at half of soil strength E_{50} based on CPT cone resistance are proposed. These formulae well reproduce $H - y_g$ response and the profiles of pile displacements and bending moments in both field loading tests and centrifuge model tests.

2. It is found that pile responses can be reproduced by using a unique interface strength reduction factor of $R_{inter} = 0.6$ regardless of installation process, such as impact driving in field loading tests, and 1-g jacking in centrifuge model tests.

Table 4 Soil parameters for HSsmall model (Case F).

Layer No.	Unit	1	2	3	4	5	6
z_{top}	m	0	2	4	6	8	12
z_{bottom}	m	2	4	6	8	12	32
z_{ref}	m	0	2	4	6	8	12
γ_{sat}	kN/m³	15.7	15.7	15.7	15.7	15.7	15.7
c'	kPa	0.1	0.1	0.1	0.1	0.1	0.1
ϕ	°	30	30	30	30	30	30
ψ	°	0	0	0	0	0	0
G_0^{ref}	kPa	49498	66337	74833	77984	77379	80883
E_{50}^{ref}	kPa	8751	11820	13565	14649	14026	14803
E_{ur}^{ref}	kPa	26253	35459	40696	43946	42077	44409
E_s^{ref}	kPa	564	3791	7406	11474	14682	19941
E_s^{inc}	kPa/m	1598	2132	2485	1880	936	1488
$\gamma_{0.7}$	—	0.000162	0.000162	0.000162	0.000162	0.000162	0.000162
RD	%	38	38	38	38	38	38
K_0	—	0.4	0.4	0.4	0.4	0.4	0.4
ν	—	0.2	0.2	0.2	0.2	0.2	0.2
ν_s	—	0.3	0.3	0.3	0.3	0.3	0.3
ν_i	—	0.45	0.45	0.45	0.45	0.45	0.45
R_f	—	0.9525	0.9525	0.9525	0.9525	0.9525	0.9525

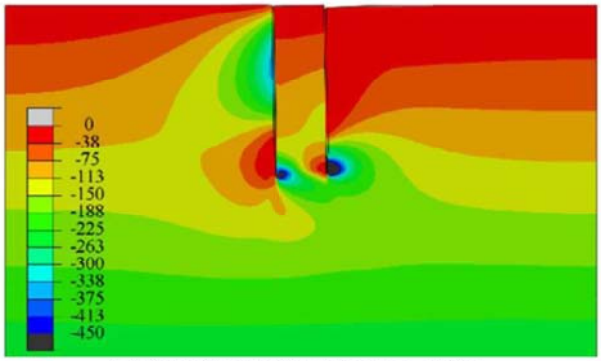

(a) 3D FEA with CEL (Fan et al., 2021).

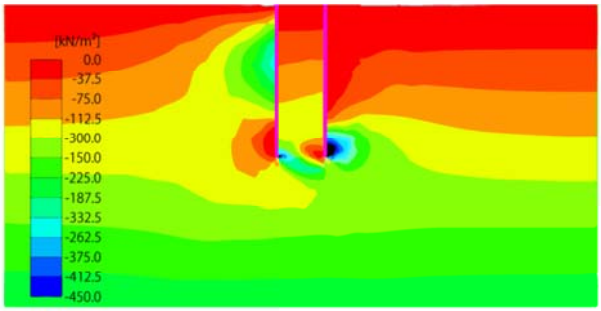

(b) 3D FEA with $R_{inter} = 0.6$ (Plaxis 3D).

Fig. 11 Comparison of principal stress σ_{11} for Case F (Load is applied from right side to left side).

ACKNOWLEDGEMENTS

This research is carried out as part of a joint program for next generation energy infrastructure The authors express their deepest gratitude to the concerned parties for their assistance during this study. The authors also thank Kazuo Takehara and Kiyomichi Yamaguchi of JIP Techno Science Corporation for their assistance with PLAXIS 3D analysis methods and Miki Sugita of Institute of Technology, Shimizu Corporation for preparing the figures.

REFERENCES

Baldi, G, Bellotti, R, Ghionna, V, Jamiolkowski, M, and Pasqualini, E (1981). "Cone resistance of a dry medium sand", *10th International Conference on Soil Mechanics and Foundation Engineering*, Stockholm, Vol. 2, pp. 427-432.

Benz, T (2007). "Small-strain stiffness of soils and its numerical consequences," *Ph.D. Thesis, Institut für Geotechnik der Universität Stuttgart*.

Brinkgreve, RBJ, Engin, E, and Engin HK (2010). "Validation of empirical formulas to derive model parameters for sands," *Numerical Methods in Geotechnical Engineering, Proceedings of 7th NUMGE*, Trondheim, Norway, CRC Press.

Burd, HJ, Taborda, DMG, Zdravković, L, Abadie, CN, Byrne, BW, Houlsby, GT, Gavin, KG, Igoe, DJP, Jardine, RJ, Martin, CM, Mcadam, RA, Pedro, AMG, and Potts, DM (2020). "PISA design model for monopiles for offshore wind turbines: application to a marine sand," *Géotechnique*, 70(11), 1048-1066.

Byrne, BW, Mcadam, RA, Burd, HJ, Houlsby, GT, Martin, CM, Beuckelaers, WJAP, Zdravković, L, Taborda, DMG, Potts, DM, Jardine, RJ, Ushev, E, Liu, T, Abadias, D, Gavin, K, Igoe, D, Doherty, P, Gretlund, JS, Andrade, MP, Wood, AM, Schroeder, FC, Turner, S, and Plummer, MAL (2017). "PISA: NEW DESIGN METHODS FOR OFFSHORE WIND TURBINE MONOPILES," *Proceedings of the 8th International Conference for Offshore Site Investigation and Geotechnics*, London, 142-161.

Fan, S, Bienen, B, and Randolph, M (2019). "Centrifuge study on effect of installation method on lateral response of monopiles in sand," *International Journal of Physical Modelling in Geotechnics*.

Fan, S, Bienen, B, and Randolph, M (2021). "Effects of Monopile Installation on Subsequent Lateral Response in Sand. II: Lateral Loading," *J. Geotech. Geoenviron. Eng.*, 147(5).

Gouw, T (2014). "Common Mistakes on the Application of Plaxis 2D in Analyzing Excavation Problems," *International Journal of Applied Engineering Research*, 9(21), 8291-8311.

Haouari, H, and Bouafia, A (2020). "A Centrifuge Modelling and Finite Element Analysis of Laterally Loaded Single Piles in Sand with Focus on P–Y Curves," *Periodica Polytechnica Civil Engineering*, 64(4), 1064-1074.

Igoe, D (2020). "3D Finite Element Modelling of Monopiles in Sand Validated Against Large Scale Field Tests," *Fourth International Symposium on Frontiers in Offshore Geotechnics*.

Igoe, D and Mohammed, MB (2022). "Application of CPT based 3DFE approach for estimating monopile damping in sand," *Cone Penetration Testing 2022*.

Mayne, PW, Coop, MR, Springman, SM, Huang, A, and Zornberg, JG (2009). "Geomaterial behavior and testing," *Proceedings of the 17th International Conference on Soil Mechanics and Geotechnical Engineering*, 2777-2872.

McAdam, RA, Byrne, BW, Houlsby, GT, Beuckelaers, WJAP, Burd, HJ, Gavin, KG, Igoe, DJP, Jardine, R, Martin, CM, Wood, AM, Potts, DM, Gretlund, JS, Taborda, DMG, and Zdravković, L (2020). "Monotonic laterally loaded pile testing in a dense marine sand at Dunkirk," *Géotechnique*, 70(11), 986-998.

Minga, E, and Burd, H (2019). "Validation of the PLAXIS MoDeTo 1D model for dense sand, Oxford University".

Nakamura, S, Matsumoto, Y, Kai, I, Iida, Y, and Ishihara, T (2023). "A study of laterally loaded monopile foundation using 1D beam models and its validation with 3D FEM analysis," *45th Wind Energy Symposium*, in Japanese.

PLAXIS 3D (2023) *PLAXIS Material Models Manual 3D, 2023.2*,Bentley.

Pedone, G, Kontoe, S, Zdravkovic, L, Jardine, RJ, Potts, DM. (2023). "A sensitivity study on the mechanical properties of interface elements adopted in finite element analyses to simulate the interaction between soil and laterally loaded piles", *10th NUMGE 2023*.

Rix, GJ, and Stokoe, KH (1991). "Correlation of Initial Tangent Modulus and Cone Penetration Resistance," *Proceedings of the First International Symposium on Calibration Chamber Testing/ISOCCTI*, 351-362.

Robertson, PK, and Campanella, RG (1983). "Interpretation of Cone Penetration Tests: Sands and Clays," *Canadian Geotechnical Journal*, 20, 719-745.

Robertson, PK, and Cabal, K (2022). *Guide to cone penetration testing 7th Edition*, Gregg Drilling LLC.

Schanz, T, Vermeer, PA, and Bonnier, PG (1999). "The hardening soil model: Formulation and Verfication," *Beyond 2000 in Computational Geotechnics*, 281-296.

Taborda, DMG, Zdravković, L, Potts, DM, Burd, HJ, Byrne, BW, Gavin, KG, Houlsby, GT, Jardine, RJ, Liu, T, Martin, CM, and McAdam, RA (2020). "Finite-element modelling of laterally loaded piles in a dense marine sand at Dunkirk," *Géotechnique*, 70(11), 1014-1029.

Trofimenkov, JG (1974). "General Reports: Eastern Europe," *Proceedings, European Symposium of Penetration Testing*, Stockholm, Sweden, Volume 2:1 General Reports, Discussions and other activities, 24-39.

Zdravković, L, Jardine, RJ, Taborda, DMG, Abadias, D, Burd, HJ, Byrne, BW, Gavin, KG, Houlsby, GT, Igoe, DJP, Liu, T, Martin, CM, Mcadam, RA, Wood, AM, Potts, DM, Gretlund, JS, Ushev, E (2020). "Ground characterization for PISA pile testing and analysis," *Géotechnique*, 70(11), 945-960.